Bias-Free in Situ H_2O_2 Generation in a Photovoltaic-Photoelectrochemical Tandem Cell for Biocatalytic Oxyfunctionalization

Choi, Da Som; Lee, Hojin; Tieves, Florian; Lee, Yang Woo; Son, Eun Jin; Zhang, Wuyuan; Shin, Byungha; Hollmann, Frank; Park, Chan Beum

DOI
10.1021/acscatal.9b04454

Publication date
2019

Document Version
Final published version

Published in
ACS Catalysis

ACS Catalysis

Letter

Cite This: ACS Catal. 2019, 9, 10562−10566

pubs.acs.org/acscatalysis

Bias-Free In Situ H_2O_2 Generation in a Photovoltaic-Photoelectrochemical Tandem Cell for Biocatalytic Oxyfunctionalization

Da Som Choi,[†] Hojin Lee,[†] Florian Tieves,[‡] Yang Woo Lee,[†] Eun Jin Son,[†] Wuyuan Zhang,[‡] Byungha Shin,[†] Frank Hollmann,[‡] and Chan Beum Park*[,†]

[†]Department of Materials Science and Engineering, Korea Advanced Institute of Science and Technology, 335 Science Road, Daejeon 34141, Republic of Korea

[‡]Department of Biotechnology, Delft University of Technology, Van der Maasweg 9, 2629HZ Delft, The Netherlands

Supporting Information

ABSTRACT: Peroxygenases catalyze selective oxyfunctionalization of hydrocarbons with high conversion efficiencies using H_2O_2 as a key cosubstrate. Here, we report an unbiased photoelectrochemical (PEC) tandem structure consisting of a FeOOH/$BiVO_4$ photoanode, a Cu(In,Ga)Se_2 solar absorber, and a graphitic carbon nitride/reduced graphene oxide hybrid cathode for light-driven peroxygenase catalysis. Powered by sufficient photovoltage generated by the solar absorber, the PEC platform generates H_2O_2 in situ through reductive activation of molecular oxygen using water as an electron donor in the absence of external bias. The peroxygenase from *Agrocybe aegerita* catalyzed the stereoselective hydroxylation of ethylbenzene to (*R*)-1-phenylethanol with total turnover numbers over 43 300 and high enantioselectivity (ee > 99%) in the unbiased PEC tandem system.

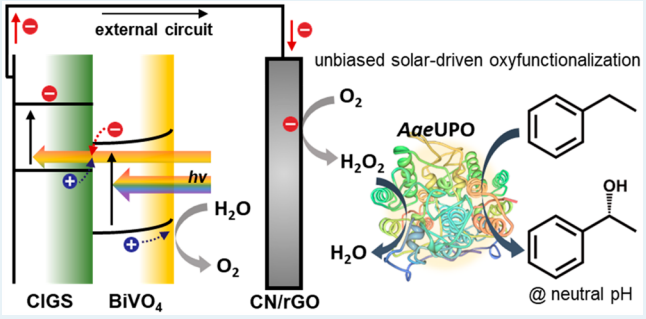

KEYWORDS: *oxyfunctionalization, photovoltaics, photoelectrochemical cells, biocatalysis, peroxygenases*

Selective oxyfunctionalization of C−H bonds remains a major challenge in organic chemistry because it requires activation of kinetically inert C−H bonds.[1] Heme-dependent oxygenases are powerful oxygenation tools due to their inherent feature of balancing reactivity with high selectivity.[2] In particular, so-called "unspecific" peroxygenases (UPOs, EC 1.11.21) have gained much interest recently because they do not rely on nicotinamide cofactors and complex electron-transfer chains to generate the catalytically active ferryl-oxo heme radical cation (compound I). They catalyze selective oxygen transfer from H_2O_2 to diverse organic substrates having nonactivated C−H bonds under mild conditions.[3] Nonetheless, UPOs suffer from oxidative degradation of the heme moiety at excess concentrations of H_2O_2.[4] To circumvent the inactivation, careful control of H_2O_2 supply is required. Stepwise addition of H_2O_2 leads to significant dilution of the reaction mixtures; thus, in situ generation of H_2O_2 through O_2 reduction is desirable to mitigate this issue.[5] To date, the most common method for the generation of H_2O_2 uses glucose oxidase,[6,7] which is not promising due to poor atom-economy (i.e., one equivalent of H_2O_2 from one equivalent of glucose) and practical issues such as high viscosity of glucose solutions. To resolve this problem, several different strategies have been proposed for in situ generation of H_2O_2 using more efficient electron donors (e.g., methanol, formate, electricity) through electrochemical,[8,9] photochemical,[10−14] or enzymatic methods.[15−17]

Here, we report a bias-free, photoelectrode−photovoltaic (PV) dual absorber tandem photoelectrochemical (PEC) platform for solar-powered in situ H_2O_2 generation coupled with peroxygenase catalysis, as depicted in Figure 1. The PEC reduction of oxygen is an economically and ecologically promising approach to produce H_2O_2 using abundant solar energy and water, avoiding the accumulation of byproducts. Moreover, physical separation of anodic and cathodic reactions in a PEC system can prevent oxidative degradation of redox enzymes and H_2O_2 oxidation at the anode.[18,19] The unassisted PEC system reduces O_2 and simultaneously generates H_2O_2 by using abundant solar energy and water in the absence of external bias. The Cu(In,Ga)Se_2 (CIGS) thin-film solar cell[20] in the PEC tandem device supply sufficient photovoltage, fulfilling the thermodynamic requirement for spontaneous PEC reaction while maximizing the fraction of solar energy collected. For solar water oxidation, we employed n-type bismuth vanadate ($BiVO_4$) that exhibits a suitable band gap (ca. 2.4 eV) and superior photochemical stability in aqueous

Received: October 15, 2019
Revised: October 18, 2019
Published: October 21, 2019

DOI: 10.1021/acscatal.9b04454
ACS Catal. 2019, 9, 10562−10566

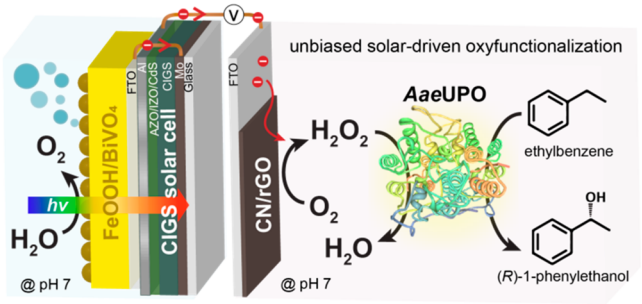

Figure 1. External bias-free, photoelectrochemical generation of H_2O_2 using water and solar energy for peroxygenase catalysis. *Aae*UPO catalyzes chemo- and stereospecific conversion of ethylbenzene to (*R*)-1-phenylethanol. In situ provision of H_2O_2 is achieved through the reduction of oxygen using FeOOH/$BiVO_4$/CIGS solar cell in tandem and CN/rGO film electrode under illumination.

environments.[21] We have paired $BiVO_4$ with CIGS solar cells to construct a PEC−PV tandem device. As a counter electrode in the PEC tandem cell, we explored the feasibility of graphitic carbon nitride (CN) and reduced graphene oxide (rGO) hybrid film[22] as an effective cathode material for O_2 reduction using electrons extracted from water oxidation at the $BiVO_4$ photoanode. CN is an attractive electrocatalyst for O_2 reduction because of its high nitrogen content, easily tunable structure, and cost-efficient production.[23] To facilitate charge transfer and increase the electrochemical active surface area, rGO is used as a supporting layer for CN. As depicted in Figure 1, the proposed tandem system generates H_2O_2 through O_2 reduction under zero applied bias, which then takes part in selective hydroxylation of ethylbenzene to (*R*)-1-phenylethanol by the recombinant peroxygenase from *Agrocybe aegerita* (*Aae*UPO).

To synthesize the CN/rGO hybrid, we casted cyanuric acid-melamine supramolecular assembly and GO aqueous dispersion blended in ethylene glycol onto a fluorine-doped SnO_2 (FTO) glass using a doctor-blade technique, followed by heating at 550 °C under a nitrogen atmosphere for 4 h according to the literature.[22] The resulting hybrids are denoted as CN/rGO-*n*, where *n* represents the weight % of GO in the precursor paste. During the calcination process, GO was thermally reduced, and a dark gray colored electrode was formed (Figure S1a). Scanning electron microscopy (SEM) (Figures S1b,c) revealed that the CN/rGO-0.2 hybrid film exhibited a porous morphology consisting of well-interconnected sheets with a thickness of approximately 40 μm. In addition, transmission electron microscopy (TEM) analysis revealed a layered nanostructure consisted of rGO and CN sheets (Figure S2). We investigated the composition and chemical structure of CN/rGO using X-ray photoelectron spectroscopy (XPS). The high-resolution N 1s spectrum of CN/rGO-0.2 (Figure S3a) was deconvoluted into three typical peaks for pyridinic N (C−N = C) at 398.7 eV, tertiary N (N−$(C)_3$) at 400.1 eV, and amino groups (C−N−H) at 401.4 eV, confirming the formation of CNs.[24] The minor peak centered at 404.2 eV corresponded to the charging effect (or π excitation) in the heterocycles.[25] With regard to the C 1s spectrum of CN/rGO-0.2, there were mainly two carbon states including C−C bonds at 284.6 eV and sp^2-bonded carbon coordination (N−C═N) at 288.5 eV (Figure S3b). Besides, two minor peaks at 285.4 and 286.1 eV corresponded to C−OH (from rGO) and C−O−C/C−O−N, respectively. C−O−N bonds play a role in the covalent bonding between the amine groups from CN and the hydroxyl (or carboxyl) groups from GO.[22] The coupling between CN and rGO was further confirmed by Fourier transform infrared spectroscopy (FTIR) (Figure S4). The breathing mode of the triazine unit shifted from 810 to 812 cm^{-1} because of the strong interaction between CN and rGO.

We evaluated CN/rGO-*n* hybrid's electrocatalytic activity for O_2 reduction by cyclic voltammetry (CV) in N_2 or O_2-saturated 0.1 M KPi buffers with a scan rate of 50 mV s^{-1} (Figure 2a, Figure S5). All CN/rGO-*n* films exhibited

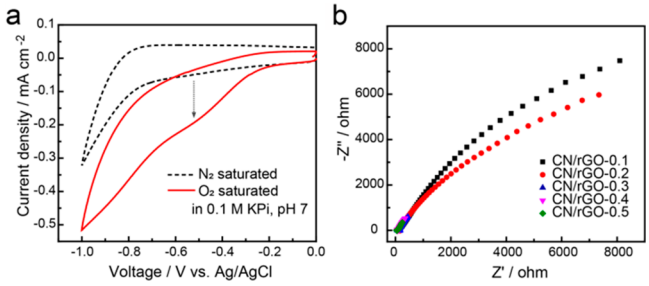

Figure 2. (a) CV curves of the CN/rGO-0.2 electrode measured in N_2- or O_2-saturated 0.1 M KPi buffer (pH 7.0) at a scan rate of 50 mV s^{-1}. (b) Nyquist curves of CN/rGO-*n* electrodes measured in a 0.1 M KPi buffer (pH 7.0) at an applied bias of −0.3 V (vs Ag/AgCl). All electrodes had a geometrical surface area of 2 cm^2.

significantly increased cathodic currents in O_2-saturated solutions compared to the currents generated in a N_2-saturated solution suggesting cathodic O_2 reduction. Increasing the amount of GO increased the peak current density of CN/rGO-*n* from −0.2 mA cm^{-2} (for CN/rGO-0.2) to −0.53 mA cm^{-2} (for CN/rGO-0.5) (Figure S5). However, the increase in the reduction current from CN/rGO-0.4 to CN/rGO-0.5 was not clearly observed. This tendency is attributed to the presence of excess rGO that could block the sites available for O_2 adsorption. Similarly, double-layer capacitance increase was observed with the increasing GO content. As shown in Figure S6, the estimated double-layer capacitance value of CN/rGO-0.5 was 29 times higher than that of CN/rGO-0.1. The sheer increase in double-layer capacitance indicates that the incorporation of rGO enhanced the electrical conductivity and the specific surface area of CN/rGO hybrid.[26] We investigated the effect of rGO on charge separation efficiency by performing electrochemical impedance spectroscopy (EIS) measurements for CN/rGO-*n* in 0.1 M KPi buffer (Figure 2b, Figure S7). The charge transfer resistance of CN/rGO-*n* film was evaluated by the semicircle diameter in the high frequency region of the Nyquist plots. The arc radius of the semicircles decreased drastically with higher loading of GO from 0.1 to 0.5 wt %, indicating the decrease in charge transfer resistance. The result shows that rGO acts as an electron conductive channel to facilitate efficient electron transfer to the solution.

We assembled a FeOOH/$BiVO_4$ photoanode and a CIGS solar cell in a tandem manner to drive unassisted H_2O_2 generation under illumination. We prepared a nanoporous $BiVO_4$ film (active area: 4 cm^2) on a FTO substrate according to the literature,[27] then photoelectrochemically deposited FeOOH as a cocatalyst on the $BiVO_4$ photoelectrode to promote the PEC activities of $BiVO_4$ toward water oxidation. $BiVO_4$ formed a nanostructure where particles of approximately 200−300 nm diameter were interconnected each other

DOI: 10.1021/acscatal.9b04454
ACS Catal. 2019, 9, 10562−10566

(Figure S8a). The band gap energy for the nanostructured FeOOH/$BiVO_4$ was estimated to be approximately 2.5 eV (Tauc plot, Figure S8b). In contrast, the CIGS solar cell possessed a band gap energy of around 1.1 eV;[28] thus, it can utilize the longer-wavelength (<1.13 mm) photons that are transmitted through the front FeOOH/$BiVO_4$ photoanode. To confirm the existence of FeOOH layer, we carried out XPS analysis on $BiVO_4$ and FeOOH/$BiVO_4$ (Figure S9). After the photoelectrodeposition of FeOOH, Fe 2p peaks and a strong peak for hydroxyl group at 530 eV in the O 1s spectrum appeared, consistent with the literature.[29]

The $J-V$ performances of the FeOOH/$BiVO_4$ photoanode and the CIGS solar cell under filtered illumination via the FeOOH/$BiVO_4$ are shown in Figure 3a. The theoretical

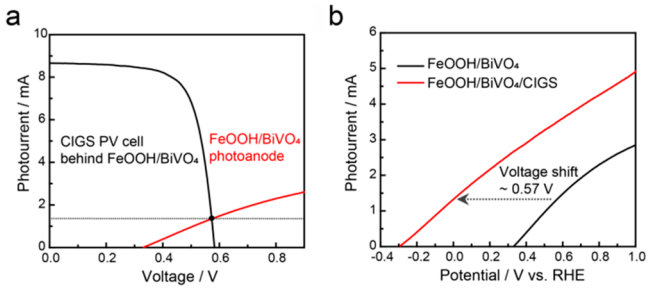

Figure 3. (a) $J-V$ curves for CIGS PV cell with FeOOH/$BiVO_4$ placed in front (black) and FeOOH/$BiVO_4$ photoanode (red) under illumination (AM 1.5G, 100 mW cm^{-2}), where the currents are based on actual areas of each components without normalization. The intersection point of two curves indicates a theoretical operating current of the tandem device. (b) Linear sweep voltammetry curves of the FeOOH/$BiVO_4$ photoanode (black) and the FeOOH/$BiVO_4$/CIGS tandem device (red) measured in 0.1 M KPi buffer (pH 7.0) at a scan rate of 50 mV s^{-1} under illumination.

operating current of the tandem system was estimated to be 1.35 mA from the photocurrent at the intersection of individual $J-V$ curves of the photoanode and the solar cell. This value is close to the actual photocurrent (1.34 mA) measured from the linear sweep voltammetric analysis of the assembled tandem device in a three-electrode configuration (Figure 3b).

We applied the CN/rGO cathode to the tandem system consisting of the FeOOH/$BiVO_4$ photoanode and the CIGS solar cell for in situ H_2O_2 generation driven by solar energy using water as an electron donor. To prevent possible oxidation of H_2O_2 at the anode, we utilized a two-chamber setup in which FeOOH/$BiVO_4$/CIGS in tandem and CN/rGO cathode were placed in different reaction vessels connected by a salt bridge. Under this configuration, the photocurrent was reduced to 40% of the value obtained from the one-chamber setup due to salt bridge's ionic resistance (Figure S10).[30] The photocurrent generated by the tandem system in a two-compartment setup was stabilized at 0.46 mA for ~14 h under illumination. To facilitate mass transfer of dissolved O_2, we gently bubbled O_2 gas into the electrolyte solution of the cathodic compartment during the experiments.[31] As shown in Figure 4a, we observed H_2O_2 generation by the PEC tandem platform, which reached a plateau of 6.5 mM after 2 h, which is 8.9-fold higher than a control experiment without CIGS solar absorber. The result indicates that an efficient production of H_2O_2 at CN/rGO electrode can be achieved in the absence of external bias by employing CIGS

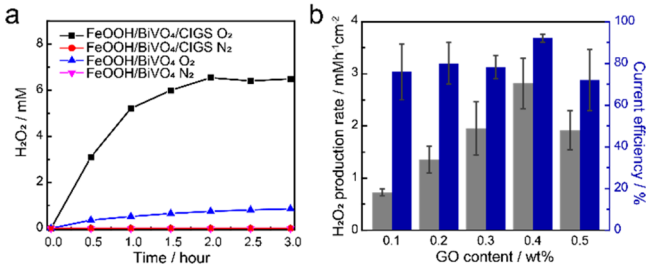

Figure 4. (a) Bias-free photoelectrochemical in situ H_2O_2 formation over CN/rGO-0.3 cathode with FeOOH/$BiVO_4$/CIGS tandem device or FeOOH/$BiVO_4$ photoanode under O_2- or N_2-purging. (b) H_2O_2 formation rates and current efficiencies by the tandem system under O_2-purging as a function of GO loading amount (wt %). H_2O_2 production rates are divided by the geometrical surface area of the electrodes.

PV cell that provides sufficient photovoltage to reduce O_2. In the absence of oxygen, no H_2O_2 generation was observed consistent with the proposed reduction of O_2. To evaluate the effect of the rGO content in the cathode on H_2O_2 generation, we measured initial production rate and current efficiency by varying the loaded GO amount from 0.1 to 0.5 wt % (Figure 4b). Consistent with the EIS and CV analysis, an increase in H_2O_2 production rate was observed with the increasing amount of GO from 0.1 to 0.4 wt %. The CN/rGO-0.4 electrode exhibited the highest H_2O_2 production rate of 2.8 mM h^{-1} cm^{-2} with a current efficiency of 92%. Higher loadings of GO (i.e., CN/rGO-0.5) did not improve the O_2-to-H_2O_2 reduction rate (1.9 mM h^{-1} cm^{-2}) showing a slight decrease of current efficiency (73%), which is attributed to the kinetic limitation by oxygen mass transfer to the cathode surface.[32] In addition, the surface nitrogen heteroatom of CN has been considered to be active sites for O_2 reduction,[33] which could be blocked by the formation of rGO at high content of GO,[34] decreasing overall H_2O_2 production rate.

We conducted *Aae*UPO-catalyzed stereospecific hydroxylation of ethylbenzene to (*R*)-1-phenylethanol as a model reaction using the PEC tandem platform (Figure 5a). With the unassisted H_2O_2 generation in the PEC tandem device, we observed a (*R*)-1-phenylethanol formation at a rate of 0.89 mM h^{-1}, which was 4.2 times faster than in the absence of CIGS solar cell. The optical purity of the product exceeded 99% enantiomeric excess (ee) in all cases, indicating the conversion was catalyzed by the enzyme. Note that (*R*)-1-

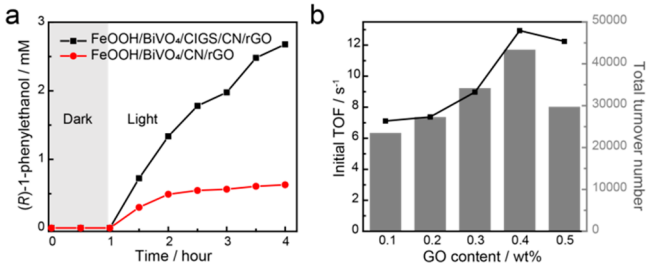

Figure 5. (a) Time profile of ethylbenzene conversion to (*R*)-1-phenylethanol by *Aae*UPO in the tandem configuration and in the absence of CIGS solar cell. (b) Influence of GO concentration on initial TOF and TTN of *Aae*UPO-catalyzed ethylbenzene hydroxylation driven by the proposed PEC tandem system. Reaction conditions: 0.1 M KPi buffer (pH 7.0, 1 mL) containing 200 nM *Aae*UPO and 100 mM ethylbenzene; 100 mW cm^{-2}; 25 °C.

DOI: 10.1021/acscatal.9b04454
ACS Catal. 2019, 9, 10562−10566

phenylethanol was not produced at all in the absence of any key component (e.g., light, oxygen, or *Aae*UPO). We further examined the effect of rGO content in the CN/rGO cathode on the performance of *Aae*UPO-catalyzed oxyfunctionalization in terms of turnover frequency (TOF) and total turnover number (TTN). In agreement with the H_2O_2 production rate, the initial TOF_{AaeUPO} and TTN_{AaeUPO} also increased with the incorporation of rGO. As shown in Figure 5b, CN/rGO-0.4 exhibited the best performance in terms of reaction rate with a TOF_{AaeUPO} of 12.9 s^{-1} and had the highest TTN_{AaeUPO} of 43 300. The TOF value is much higher compared with other PEC platforms for in situ H_2O_2 generation such as flavin-hybridized carbon nanotube photocathode (TOF: 1 s^{-1}).[35] Additionally, a further increase of the GO loading lowered the biocatalytic conversion; initial TOF_{AaeUPO} of 12.2 s^{-1} and the TTN_{AaeUPO} of 29 700 were observed for CN/rGO-0.5. The decrease in the TTN with CN/rGO-0.5 may be caused by excess electrons provided by the highly conductive CN/rGO film, and possibly, hydroxyl radicals originating from H_2O_2 reduction [E (H_2O_2/·OH) = 0.38 V vs NHE, pH 7] cause oxidative inactivation of *Aae*UPO (Figure S11). According to the literature,[36] hydroxyl radicals among reactive oxygen species can directly attack the active site of *Aae*UPO. Using the CN/rGO-0.5 cathode, product formation ceased within 4 h (Figure S12), which we ascribed to biocatalyst deactivation. The results suggest that careful control of rGO amount is essential to sustain activity of *Aae*UPO, while suppressing undesired side reactions. We further explored the substrate scope of photoelectroenzymatic hydroxylation in the tandem PEC system. As listed in Table S1, a broad range of aromatic compounds were converted into their corresponding alcohols. Taken together, the deliberate integration of the PEC−PV tandem device with *Aae*UPO can produce fine and specialty chemicals without any external energy supply in pursuit of a higher efficiency, while the previously reported PEC method[35] requires an additional bias of −0.4 V (vs Ag/AgCl) in addition to the light energy to promote optimized UPO reactions. We envision that a further increase of turnover numbers can be achieved by enhancing enzyme stability through the use of hydroxyl radical scavengers and physical separation of *Aae*UPO from the electrode.

In summary, we successfully demonstrated peroxygenase-catalyzed oxyfunctionalization of C−H bonds through unbiased photoelectrochemical H_2O_2 generation using a PEC tandem cell structure consisted of a FeOOH/$BiVO_4$ photoanode, a CIGS solar cell, and a CN/rGO cathode. The single-pass tandem configuration allows for the well-managed light harvesting and provides sufficient energy to drive water oxidation at the FeOOH/$BiVO_4$ and simultaneous O_2 reduction at the cathode under no external bias. The CN/rGO cathode having significantly enhanced electrical conductivity and effective surface area owing to rGO allowed for high oxygen reduction activity. By integrating the CN/rGO-0.4 cathode to the PEC tandem cell, H_2O_2 was generated at a rate of 2.8 mM h^{-1} cm^{-2} under visible light in the absence of external bias. Finally, we successfully achieved photoelectroenzymatic hydroxylation of ethylbenzene to enantiopure (*R*)-1-phenylethanol with a TTN of 43 300 and a TOF of 12.9 s^{-1} in the tandem platform. Our approach suggests that careful integration of unbiased PEC system with peroxygenases can promote C−H oxyfunctionalization using solar-powered electrons extracted from water.

■ ASSOCIATED CONTENT

Supporting Information

The Supporting Information is available free of charge on the ACS Publications website at DOI: 10.1021/acscatal.9b04454.

Experimental procedures, SEM, TEM, XPS, FTIR, and electrochemical characterization (PDF)

■ AUTHOR INFORMATION

Corresponding Author

*E-mail for C.B.P.: parkcb@kaist.ac.kr.

ORCID

Wuyuan Zhang: 0000-0002-3182-5107
Byungha Shin: 0000-0001-6845-0305
Frank Hollmann: 0000-0003-4821-756X
Chan Beum Park: 0000-0002-0767-8629

Notes

The authors declare no competing financial interest.

■ ACKNOWLEDGMENTS

This work was supported by the National Research Foundation (NRF) via the Creative Research Initiative Center (grant number: NRF-2015 R1A3A2066191), Republic of Korea.

■ REFERENCES

(1) Xue, X.-S.; Ji, P.; Zhou, B.; Cheng, J.-P. The Essential Role of Bond Energetics in C−H Activation/Functionalization. *Chem. Rev.* **2017**, *117*, 8622−8648.

(2) Dong, J.; Fernández-Fueyo, E.; Hollmann, F.; Paul, C. E.; Pesic, M.; Schmidt, S.; Wang, Y.; Younes, S.; Zhang, W. Biocatalytic Oxidation Reactions: A Chemist's Perspective. *Angew. Chem., Int. Ed.* **2018**, *57*, 9238−9261.

(3) Wang, Y.; Lan, D.; Durrani, R.; Hollmann, F. Peroxygenases en route to Becoming Dream Catalysts. What Are the Opportunities and Challenges? *Curr. Opin. Chem. Biol.* **2017**, *37*, 1−9.

(4) Bormann, S.; Gomez Baraibar, A.; Ni, Y.; Holtmann, D.; Hollmann, F. Specific Oxyfunctionalisations Catalysed by Peroxygenases: Opportunities, Challenges and Solutions. *Catal. Sci. Technol.* **2015**, *5*, 2038−2052.

(5) Burek, B. O.; Bormann, S.; Hollmann, F.; Bloh, J. Z.; Holtmann, D. Hydrogen Peroxide Driven Biocatalysis. *Green Chem.* **2019**, *21*, 3232−3249.

(6) Bankar, S. B.; Bule, M. V.; Singhal, R. S.; Ananthanarayan, L. Glucose Oxidase — An Overview. *Biotechnol. Adv.* **2009**, *27*, 489−501.

(7) Pereira, P. C.; Arends, I. W. C. E.; Sheldon, R. A. Optimizing the Chloroperoxidase−Glucose Oxidase System: The Effect of Glucose Oxidase on Activity and Enantioselectivity. *Process Biochem.* **2015**, *50*, 746−751.

(8) Horst, A. E. W.; Bormann, S.; Meyer, J.; Steinhagen, M.; Ludwig, R.; Drews, A.; Ansorge-Schumacher, M.; Holtmann, D. Electro-Enzymatic Hydroxylation of Ethylbenzene by the Evolved Unspecific Peroxygenase of Agrocybe Aegerita. *J. Mol. Catal. B: Enzym.* **2016**, *133*, S137−S142.

(9) Getrey, L.; Krieg, T.; Hollmann, F.; Schrader, J.; Holtmann, D. Enzymatic Halogenation of the Phenolic Monoterpenes Thymol and Carvacrol with Chloroperoxidase. *Green Chem.* **2014**, *16*, 1104−1108.

(10) Churakova, E.; Kluge, M.; Ullrich, R.; Arends, I.; Hofrichter, M.; Hollmann, F. Specific Photobiocatalytic Oxyfunctionalization Reactions. *Angew. Chem., Int. Ed.* **2011**, *50*, 10716−10719.

(11) Zhang, W.; Burek, B. O.; Fernández-Fueyo, E.; Alcalde, M.; Bloh, J. Z.; Hollmann, F. Selective Activation of C−H Bonds in a Cascade Process Combining Photochemistry and Biocatalysis. *Angew. Chem., Int. Ed.* **2017**, *56*, 15451−15455.

DOI: 10.1021/acscatal.9b04454
ACS Catal. 2019, 9, 10562−10566

(12) Zhang, W.; Fernández-Fueyo, E.; Ni, Y.; van Schie, M.; Gacs, J.; Renirie, R.; Wever, R.; Mutti, F. G.; Rother, D.; Alcalde, M.; Hollmann, F. Selective Aerobic Oxidation Reactions Using a Combination of Photocatalytic Water Oxidation and Enzymatic Oxyfunctionalizations. *Nat. Catal.* **2018**, *1*, 55−62.
(13) Seel, C. J.; Králík, A.; Hacker, M.; Frank, A.; König, B.; Gulder, T. Atom-Economic Electron Donors for Photobiocatalytic Halogenations. *ChemCatChem* **2018**, *10*, 3960−3963.
(14) Willot, S. J. P.; Fernández-Fueyo, E.; Tieves, F.; Pesic, M.; Alcalde, M.; Arends, I. W. C. E.; Park, C. B.; Hollmann, F. Expanding the Spectrum of Light-Driven Peroxygenase Reactions. *ACS Catal.* **2019**, *9*, 890−894.
(15) Ni, Y.; Fernández-Fueyo, E.; Baraibar, A. G.; Ullrich, R.; Hofrichter, M.; Yanase, H.; Alcalde, M.; van Berkel, W. J. H.; Hollmann, F. Peroxygenase-Catalyzed Oxyfunctionalization Reactions Promoted by the Complete Oxidation of Methanol. *Angew. Chem., Int. Ed.* **2016**, *55*, 798−801.
(16) Tieves, F.; Willot, S. J.-P.; van Schie, M. M. C. H.; Rauch, M. C. R.; Younes, S. H. H.; Zhang, W.; Dong, J.; Gomez de Santos, P.; Robbins, J. M.; Bommarius, B.; Alcalde, M.; Bommarius, A. S.; Hollmann, F. Formate Oxidase (FOx) from Aspergillus oryzae: One Catalyst Enables Diverse H_2O_2-Dependent Biocatalytic Oxidation Reactions. *Angew. Chem., Int. Ed.* **2019**, *58*, 7873−7877.
(17) Rocha-Martin, J.; Velasco-Lozano, S.; Guisán, J. M.; López-Gallego, F. Oxidation of Phenolic Compounds Catalyzed by Immobilized Multi-Enzyme Systems with Integrated Hydrogen Peroxide Production. *Green Chem.* **2014**, *16*, 303−311.
(18) Kim, J.; Park, C. B. Shedding Light on Biocatalysis: Photoelectrochemical Platforms for Solar-Driven Biotransformation. *Curr. Opin. Chem. Biol.* **2019**, *49*, 122−129.
(19) Lee, S. H.; Choi, D. S.; Kuk, S. K.; Park, C. B. Photobiocatalysis: Activating Redox Enzymes by Direct or Indirect Transfer of Photoinduced Electrons. *Angew. Chem., Int. Ed.* **2018**, *57*, 7958−7985.
(20) Kim, S. T.; Larina, L.; Yun, J. H.; Shin, B.; Ahn, B. T. Surface Passivation and Point Defect Control in Cu(In,Ga)Se_2 Films with a Na_2S Post Deposition Treatment for Higher Than 19% CIGS Cell Performance. *Sustain. Energy Fuels* **2019**, *3*, 709−716.
(21) Kang, D.; Kim, T. W.; Kubota, S. R.; Cardiel, A. C.; Cha, H. G.; Choi, K.-S. Electrochemical Synthesis of Photoelectrodes and Catalysts for Use in Solar Water Splitting. *Chem. Rev.* **2015**, *115*, 12839−12887.
(22) Peng, G.; Volokh, M.; Tzadikov, J.; Sun, J.; Shalom, M. Carbon Nitride/Reduced Graphene Oxide Film with Enhanced Electron Diffusion Length: An Efficient Photo-Electrochemical Cell for Hydrogen Generation. *Adv. En. Mater.* **2018**, *8*, 1800566.
(23) Niu, W.; Yang, Y. Graphitic Carbon Nitride for Electrochemical Energy Conversion and Storage. *ACS En. Lett.* **2018**, *3*, 2796−2815.
(24) Thomas, A.; Fischer, A.; Goettmann, F.; Antonietti, M.; Müller, J.-O.; Schlögl, R.; Carlsson, J. M. Graphitic Carbon Nitride Materials: Variation of Structure and Morphology and Their Use as Metal-Free Catalysts. *J. Mater. Chem.* **2008**, *18*, 4893−4908.
(25) Zhang, G.; Zhang, J.; Zhang, M.; Wang, X. Polycondensation of Thiourea into Carbon Nitride Semiconductors as Visible Light Photocatalysts. *J. Mater. Chem.* **2012**, *22*, 8083−8091.
(26) Bikkarolla, S. K.; Cumpson, P.; Joseph, P.; Papakonstantinou, P. Oxygen Reduction Reaction by Electrochemically Reduced Graphene Oxide. *Faraday Discuss.* **2014**, *173*, 415−428.
(27) Kim, T. W.; Choi, K.-S. Nanoporous $BiVO_4$ Photoanodes with Dual-Layer Oxygen Evolution Catalysts for Solar Water Splitting. *Science* **2014**, *343*, 990−994.
(28) Koo, B.; Nam, S.-W.; Haight, R.; Kim, S.; Oh, S.; Cho, M.; Oh, J.; Lee, J. Y.; Ahn, B. T.; Shin, B. Tailoring Photoelectrochemical Performance and Stability of Cu(In,Ga)Se_2 Photocathode via TiO_2-Coupled Buffer Layers. *ACS Appl. Mater. Interfaces* **2017**, *9*, 5279−5287.
(29) Son, E. J.; Lee, S. H.; Kuk, S. K.; Pesic, M.; Choi, D. S.; Ko, J. W.; Kim, K.; Hollmann, F.; Park, C. B. Carbon Nanotube−Graphitic Carbon Nitride Hybrid Films for Flavoenzyme-Catalyzed Photoelectrochemical Cells. *Adv. Funct. Mater.* **2018**, *28*, 1705232.
(30) Lee, Y. W.; Boonmongkolras, P.; Son, E. J.; Kim, J.; Lee, S. H.; Kuk, S. K.; Ko, J. W.; Shin, B.; Park, C. B. Unbiased Biocatalytic Solar-to-Chemical Conversion by FeOOH/$BiVO_4$/Perovskite Tandem Structure. *Nat. Commun.* **2018**, *9*, 4208.
(31) Shi, X.; Zhang, Y.; Siahrostami, S.; Zheng, X. Light-Driven $BiVO_4$−C Fuel Cell with Simultaneous Production of H_2O_2. *Adv. En. Mater.* **2018**, *8*, 1801158.
(32) Ma, P.; Ma, H.; Galia, A.; Sabatino, S.; Scialdone, O. Reduction of Oxygen to H_2O_2 at Carbon Felt Cathode in Undivided Cells. Effect of the Ratio Between the Anode and the Cathode Surfaces and of Other Operative Parameters. *Sep. Purif. Technol.* **2019**, *208*, 116−122.
(33) Gong, K.; Du, F.; Xia, Z.; Durstock, M.; Dai, L. Nitrogen-Doped Carbon Nanotube Arrays with High Electrocatalytic Activity for Oxygen Reduction. *Science* **2009**, *323*, 760.
(34) Tiong, P.; Lintang, H. O.; Endud, S.; Yuliati, L. Improved Interfacial Charge Transfer and Visible Light Activity of Reduced Graphene Oxide−Graphitic Carbon Nitride Photocatalysts. *RSC Adv.* **2015**, *5*, 94029−94039.
(35) Choi, D. S.; Ni, Y.; Fernández-Fueyo, E.; Lee, M.; Hollmann, F.; Park, C. B. Photoelectroenzymatic Oxyfunctionalization on Flavin-Hybridized Carbon Nanotube Electrode Platform. *ACS Catal.* **2017**, *7*, 1563−1567.
(36) Burek, B. O.; de Boer, S. R.; Tieves, F.; Zhang, W.; van Schie, M.; Bormann, S.; Alcalde, M.; Holtmann, D.; Hollmann, F.; Bahnemann, D. W.; Bloh, J. Z. Photoenzymatic Hydroxylation of Ethylbenzene Catalyzed by Unspecific Peroxygenase: Origin of Enzyme Inactivation and the Impact of Light Intensity and Temperature. *ChemCatChem* **2019**, *11*, 3093−3100.

DOI: 10.1021/acscatal.9b04454
ACS Catal. 2019, 9, 10562−10566